Spin susceptibility of three-dimensional Dirac-Weyl semimetals

Yuya Ominato[1] and Kentaro Nomura[1,2]
[1]*Institute for Materials Research, Tohoku University, Sendai 980-8577, Japan*
[2]*Center for Spintronics Research Network, Tohoku University, Sendai 980-8577, Japan*

(Received 31 January 2018; published 20 June 2018)

We theoretically study the spin susceptibility of Dirac semimetals using linear-response theory. The spin susceptibility is decomposed into an intraband contribution and an interband contribution. We obtain analytical expressions for the intraband and interband contributions of massless Dirac fermions. The spin susceptibility is independent of the Fermi energy, whereas it depends on the cutoff energy, which is introduced to regularize the integration. We find that the cutoff energy is appropriately determined by comparing the results for the Wilson-Dirac lattice model, which approximates the massless Dirac Hamiltonian around the Dirac point. We also calculate the spin susceptibility of massive Dirac fermions for the model of topological insulators. We discuss the effect of the band inversion and the strength of spin-orbit coupling.

DOI: 10.1103/PhysRevB.97.245207

I. INTRODUCTION

Topological semimetals, such as Dirac semimetals [1,2], Weyl semimetals [3–6], and nodal line semimetals [7–10], possess exotic electronic band structures, which are significantly different from conventional metals and insulators. They exhibit fascinating physical properties originating from their topologically nontrivial band structures. There are many theoretical proposals to realize topological semimetals, some of which were experimentally confirmed [11–16]. A Dirac semimetal has band touching points, and the energy bands are doubly degenerate. By breaking either inversion symmetry or time-reversal symmetry, the degeneracy is lifted, and a Dirac semimetal becomes a Weyl semimetal. The inversion broken Weyl semimetals are experimentally confirmed [14–16], and there are several materials including type-II Weyl semimetals [17]. On the other hand, there are few experimental indications for the Weyl semimetals with broken time-reversal symmetry, i.e., the magnetic Weyl semimetals [18–20], although there are many theoretical predictions [5,7,21–27].

One of the theoretical predictions to realize the magnetic Weyl semimetals is magnetically doped topological insulators [21,27–29]. Ferromagnetic ordering in topological insulators is experimentally observed [30–36]. In these systems, the ferromagnetic Weyl phase can emerge if the exchange coupling is sufficiently strong to overcome the energy gap. The magnetic properties and the topological phase transition induced by magnetic doping are characterized by the spin susceptibility of band electrons. Within the mean-field theory, a condition to exhibit the ferromagnetic ordering is given by $J^2\chi_m\chi_s > 1$ [28], where J is the exchange coupling constant, χ_m is the spin susceptibility of local magnetic moments, and χ_s is the spin susceptibility of band electrons. χ_m obeys the Curie law and is proportional to an inverse of temperature ($\chi_m \propto 1/T$). Therefore, the ferromagnetic ordering can be observed at sufficiently low temperatures as long as χ_s is finite. If the spin-orbit coupling is negligible, χ_s is proportional to the density of states, i.e., χ_s is determined by a Fermi-surface property. In the presence of the strong spin-orbit coupling, however, occupied states also give considerable contribution, and χ_s becomes finite even when the Fermi level resides in the energy gap. This is the interband effect and known as the Van Vleck paramagnetism. In the topological insulators and semimetals, the nontrivial energy band structure originates from the strong spin-orbit coupling. Therefore, the investigation of χ_s in these systems is an important issue to discuss the magnetic phase transition and the effect of the strong spin-orbit coupling.

In this paper, we study the spin susceptibility of three-dimensional Dirac semimetals within linear-response theory. The spin susceptibility is composed of the intraband contribution $\chi_{\rm intra}$ and the interband contribution $\chi_{\rm inter}$. In the presence of strong spin-orbit coupling, $\chi_{\rm inter}$ gives large contributions. The interband effect is important in the orbital diamagnetism of the Dirac fermions [37–41]. We obtain analytical expressions for the spin susceptibility of the massless Dirac fermions. The spin susceptibility is independent of Fermi energy, whereas it depends on the cutoff energy, which is introduced by hand to regularize the integration. We calculate the spin susceptibility of the Wilson-Dirac lattice model, which reduces to the massless Dirac Hamiltonian around the Γ point. We find that the cutoff energy can be related to some parameters of the lattice model and that the Fermi-energy dependence of the spin susceptibility exhibits quantitatively the same behavior in the two models. We also calculate the spin susceptibility of massive Dirac fermions, which are models of band electrons in topological insulators. The spin susceptibility is finite even in the energy gap because of strong spin-orbit coupling.

The paper is organized as follows. In Sec. II, we formulate the spin susceptibility and briefly review the qualitative behavior of the spin susceptibility in the presence of spin-orbit coupling. In Secs. III and IV, we introduce a continuum model and a lattice model which describe electronic states in a Dirac semimetal. The spin susceptibility of them is calculated. In Sec. V, we calculate the spin susceptibility of massive Dirac fermions. The conclusion is given in Sec. VI.

II. SPIN SUSCEPTIBILITY

To calculate the spin susceptibility, we introduce the Zeeman coupling between the electrons and an external magnetic field. The Hamiltonian is given by

$$H = H_0 + H_{\text{Zeeman}}, \tag{1}$$

where H_0 is an unperturbed Hamiltonian and the Zeeman term is given by

$$H_{\text{Zeeman}} = \frac{g\mu_{\text{B}}}{2}\boldsymbol{\sigma}\cdot\boldsymbol{B}, \tag{2}$$

where g is the g factor, μ_{B} is the Bohr magneton, and $\boldsymbol{\sigma}$ is the triplets of Pauli matrices acting on the real spin degree of freedom. When we discuss the ferromagnetic ordering based on χ_s, the g factor should be set to $g = 2$. In the following, however, we formulate and calculate the spin susceptibility with an arbitrary value of the g factor. This is for applicability our results to magnetic response where the g factor is modulated by the orbital effect [42].

We apply an external magnetic field with infinitely slow spatial variation,

$$\boldsymbol{B} = [0,0,B\,\cos(\boldsymbol{q}\cdot\boldsymbol{r})]. \tag{3}$$

The slow spatial variation of the field is controlled by the wave-vector $\boldsymbol{q}$, which will tend to zero at the end of the calculation. Within the linear response, the induced magnetization is given by

$$M(\boldsymbol{r}) = \chi_s(\boldsymbol{q})B\,\cos(\boldsymbol{q}\cdot\boldsymbol{r}), \tag{4}$$

where the spin susceptibility $\chi_s(\boldsymbol{q})$ is obtained as

$$\chi_s(\boldsymbol{q},\mu,T) = \frac{1}{V}\sum_{nm\boldsymbol{k}}\frac{-f_{n\boldsymbol{k}}(\mu,T)+f_{m\boldsymbol{k}-\boldsymbol{q}}(\mu,T)}{\varepsilon_{n\boldsymbol{k}}-\varepsilon_{m\boldsymbol{k}-\boldsymbol{q}}} \times\left|\langle n,\boldsymbol{k}|\frac{g\mu_{\text{B}}}{2}\sigma_z|m,\boldsymbol{k}-\boldsymbol{q}\rangle\right|^2, \tag{5}$$

where μ is the chemical potential, T is the temperature, V is the volume of the system, $f_{n\boldsymbol{k}}(\mu,T)$ is the Fermi distribution function, $|n,\boldsymbol{k}\rangle$ is a Bloch state of the unperturbed Hamiltonian, and $\varepsilon_{n\boldsymbol{k}}$ is its energy eigenvalue. Taking the long-wavelength limit $|\boldsymbol{q}|\to 0$, we obtain

$$\lim_{|\boldsymbol{q}|\to 0}\chi_s(\boldsymbol{q},\mu,T) = \int_{-\infty}^{\infty}d\varepsilon\left(-\frac{\partial f(\mu,T)}{\partial\varepsilon}\right)\chi_s(\varepsilon_{\text{F}}), \tag{6}$$

where $\chi_s(\varepsilon_{\text{F}})$ is the spin susceptibility at $T = 0$ and decomposed into

$$\chi_s(\varepsilon_{\text{F}}) = \chi_{\text{intra}}(\varepsilon_{\text{F}}) + \chi_{\text{inter}}(\varepsilon_{\text{F}}), \tag{7}$$

where $\chi_{\text{intra}}(\varepsilon_{\text{F}})$ is the intraband contribution,

$$\chi_{\text{intra}}(\varepsilon_{\text{F}}) = \frac{1}{V}\sum_{n\boldsymbol{k}}\delta(\varepsilon_{n\boldsymbol{k}}-\varepsilon_{\text{F}})\left|\langle n,\boldsymbol{k}|\frac{g\mu_{\text{B}}}{2}\sigma_z|n,\boldsymbol{k}\rangle\right|^2, \tag{8}$$

and $\chi_{\text{inter}}(\varepsilon_{\text{F}})$ is the interband contribution,

$$\chi_{\text{inter}}(\varepsilon_{\text{F}}) = \frac{1}{V}\sum_{n\neq m\boldsymbol{k}}\frac{-\theta(\varepsilon_{\text{F}}-\varepsilon_{n\boldsymbol{k}})+\theta(\varepsilon_{\text{F}}-\varepsilon_{m\boldsymbol{k}})}{\varepsilon_{n\boldsymbol{k}}-\varepsilon_{m\boldsymbol{k}}} \times\left|\langle n,\boldsymbol{k}|\frac{g\mu_{\text{B}}}{2}\sigma_z|m,\boldsymbol{k}\rangle\right|^2. \tag{9}$$

where $\theta(\varepsilon)$ is the Heaviside step function. At $T = 0$, only electronic states on the Fermi surface contribute to χ_{intra}. On the other hand, all electronic states below the Fermi energy can contribute to χ_{inter}. In order to get a finite χ_{inter}, the commutation relation between the Hamiltonian and the spin operator has to be nonzero,

$$[H_0,\sigma_z]\neq 0. \tag{10}$$

If the commutation relation is zero, the matrix elements in Eq. (9) vanish, and χ_{inter} becomes zero. In the presence of the strong spin-orbit coupling, χ_{inter} gives a large contribution.

III. CONTINUUM DIRAC FERMION MODEL

We consider a model Hamiltonian for electrons in Dirac semimetals,

$$H_{\text{continuum}} = \hbar v\tau_z\boldsymbol{\sigma}\cdot\boldsymbol{k}, \tag{11}$$

where v is the velocity and $\boldsymbol{\sigma}$ and $\boldsymbol{\tau}$ are the triplets of Pauli matrices acting on the real spin and the pseudospin (chirality) degrees of freedom. We calculate the spin susceptibility of the above model. In the present model, the chirality is a good quantum number so that the chirality degrees of freedom just double the spin susceptibility. Therefore, following calculation is equally applicable to the Weyl Hamiltonian. The eigenstates of the Hamiltonian with positive chirality are given by

$$|+,\boldsymbol{k}\rangle = \begin{pmatrix}\cos(\theta_{\boldsymbol{k}}/2)e^{-i\phi_{\boldsymbol{k}}/2}\\ \sin(\theta_{\boldsymbol{k}}/2)e^{i\phi_{\boldsymbol{k}}/2}\end{pmatrix}, \tag{12}$$

$$|-,\boldsymbol{k}\rangle = \begin{pmatrix}-\sin(\theta_{\boldsymbol{k}}/2)e^{-i\phi_{\boldsymbol{k}}/2}\\ \cos(\theta_{\boldsymbol{k}}/2)e^{i\phi_{\boldsymbol{k}}/2}\end{pmatrix}, \tag{13}$$

where $|s,\boldsymbol{k}\rangle$ is the eigenstate with the energy,

$$\varepsilon_{s\boldsymbol{k}} = s\hbar vk, \tag{14}$$

where $k = \sqrt{k_x^2+k_y^2+k_z^2}$ and $s = \pm 1$. $\theta_{\boldsymbol{k}}$ and $\phi_{\boldsymbol{k}}$ are the zenith and azimuth angles of the wave-vector $\boldsymbol{k}$.

The intraband and interband matrix elements are calculated as

$$\left|\langle s,\boldsymbol{k}|\frac{g\mu_{\text{B}}}{2}\sigma_z|s,\boldsymbol{k}\rangle\right|^2 = \left(\frac{g\mu_{\text{B}}}{2}\right)^2\cos^2\theta_{\boldsymbol{k}}, \tag{15}$$

$$\left|\langle -s,\boldsymbol{k}|\frac{g\mu_{\text{B}}}{2}\sigma_z|s,\boldsymbol{k}\rangle\right|^2 = \left(\frac{g\mu_{\text{B}}}{2}\right)^2\sin^2\theta_{\boldsymbol{k}}. \tag{16}$$

We obtain an analytical expression for χ_{intra},

$$\chi_{\text{intra}}(\varepsilon_{\text{F}}) = \frac{1}{3\pi^2}\left(\frac{g\mu_{\text{B}}}{2}\right)^2\frac{\varepsilon_{\text{F}}^2}{(\hbar v)^3}, \tag{17}$$

where $\varepsilon_{\text{F}} = \hbar vk_{\text{F}}$ is the Fermi energy. χ_{intra} is proportional to the density of states $D(\varepsilon_{\text{F}})$,

$$D(\varepsilon_{\text{F}}) = \frac{\varepsilon_{\text{F}}^2}{\pi^2(\hbar v)^3}, \tag{18}$$

and corresponds to Pauli paramagnetism [43]. The interband contribution χ_{inter} is also calculated analytically,

$$\chi_{\text{inter}}(\varepsilon_{\text{F}}) = \frac{1}{3\pi^2}\left(\frac{g\mu_{\text{B}}}{2}\right)^2\frac{\varepsilon_{\text{c}}^2-\varepsilon_{\text{F}}^2}{(\hbar v)^3}, \tag{19}$$

where $\varepsilon_c = \hbar v k_c$ is a cutoff energy. This corresponds to the Van Vleck paramagnetism [28,34]. In the present model, there are infinite states below the Fermi energy so that we introduce a spherical cutoff with the radius k_c in order to regularize the integration by $\boldsymbol{k}$.

The spin susceptibility χ_s, which is the sum of $\chi_{\rm intra}$ and $\chi_{\rm inter}$, is obtained as

$$\chi_s(\varepsilon_F) = \frac{1}{3\pi^2}\left(\frac{g\mu_B}{2}\right)^2 \frac{\varepsilon_c^2}{(\hbar v)^3}. \tag{20}$$

There are two important features. First, the spin susceptibility is independent of the Fermi energy [41] because the Fermi-energy-dependent terms of $\chi_{\rm intra}$ and $\chi_{\rm inter}$ exactly cancel each other. Therefore, the spin susceptibility is independent of the temperature as we can see in Eq. (6). Second, the spin susceptibility is proportional to ε_c^2 [44]. The spin susceptibility of surface states in three-dimensional topological insulators, i.e., two-dimensional massless Dirac fermions, depends on the cutoff energy linearly [45–47]. We can show the linear cutoff dependence of the spin susceptibility in two-dimensional massless Dirac fermions for the in-plane direction, i.e., the x-y direction. On the other hand, the orbital magnetic susceptibility logarithmically diverges at the Dirac point [37,39–41] and decreases off the Dirac point. Therefore, the spin susceptibility can dominate over the orbital contribution off the Dirac point.

We mention two remarks on the spin susceptibility Eq. (20). First, the cutoff energy ε_c is introduced by hand and cannot be determined within the continuum model scheme. Second, we consider the continuum model and introduce the cutoff energy ε_c, which means the omission of the interband contribution from the electronic states below the cutoff energy. This contribution can give a constant offset for the spin susceptibility [41]. Equation (20) does not include the offset. In the following section, we address these two remarks.

IV. LATTICE DIRAC FERMION MODEL

In this section, we calculate the spin susceptibility of the Wilson-Dirac-type cubic lattice model,

$$\begin{aligned} H_{\rm Lattice} &= t\tau_z \sum_{i=x,y,z} \sigma_i \sin k_i a + m_{\boldsymbol{k}}\tau_x, \\ m_{\boldsymbol{k}} &= m \sum_{i=x,y,z} (1-\cos k_i a), \end{aligned} \tag{21}$$

where $\hbar v k_i (i=x,y,z)$ in Eq. (11) is simply replaced by $t \sin k_i a$ with the hopping energy t and the lattice spacing a and these parameters are related as

$$\hbar v = ta. \tag{22}$$

The second term $m_{\boldsymbol{k}}\tau_x$ is introduced to gap out the point nodes other than the origin $(k_x,k_y,k_z) = (0,0,0)$. In the vicinity of the origin, Eq. (22) approximates the continuum model Eq. (11) within the first order of k_i. The eigenstates of the lattice model are given by

$$|R,s,\boldsymbol{k}\rangle = \frac{1}{\sqrt{2\varepsilon_{s\boldsymbol{k}}(\varepsilon_{s\boldsymbol{k}} - t\sin k_z a)}} \begin{pmatrix} t(\sin k_x a - i \sin k_y a) \\ \varepsilon_{s\boldsymbol{k}} - t\sin k_z a \\ 0 \\ m_{\boldsymbol{k}} \end{pmatrix}, \tag{23}$$

$$|L,s,\boldsymbol{k}\rangle = \frac{1}{\sqrt{2\varepsilon_{s\boldsymbol{k}}(\varepsilon_{s\boldsymbol{k}} - t\sin k_z a)}} \begin{pmatrix} -m_{\boldsymbol{k}} \\ 0 \\ -\varepsilon_{s\boldsymbol{k}} + t\sin k_z a \\ t(\sin k_x a + i \sin k_y a) \end{pmatrix}, \tag{24}$$

where $\varepsilon_{s\boldsymbol{k}} = s\sqrt{t^2(\sin^2 k_x a + \sin^2 k_y a + \sin^2 k_z a) + m_{\boldsymbol{k}}^2}$ and $s = \pm 1$. $|R,s,\boldsymbol{k}\rangle$ and $|L,s,\boldsymbol{k}\rangle$ correspond to the eigenstates of the continuum model with positive and negative chiralities. The intraband matrix elements are calculated as

$$\begin{aligned} &\sum_{\alpha\beta s} \delta(\varepsilon_{s\boldsymbol{k}} - \varepsilon_F) \left| \langle \alpha,s,\boldsymbol{k}| \frac{g\mu_B}{2}\sigma_z |\beta,s,\boldsymbol{k}\rangle \right|^2 \\ &= \sum_s \delta(\varepsilon_{s\boldsymbol{k}} - \varepsilon_F) \left(\frac{g\mu_B}{2}\right)^2 \frac{2(t^2 \sin^2 k_z a + m_{\boldsymbol{k}}^2)}{\varepsilon_{s\boldsymbol{k}}^2}, \end{aligned} \tag{25}$$

and the interband matrix elements are

$$\begin{aligned} &\sum_{\alpha\beta s} \frac{-\theta(\varepsilon_F - \varepsilon_{s\boldsymbol{k}}) + \theta(\varepsilon_F - \varepsilon_{-s\boldsymbol{k}})}{\varepsilon_{s\boldsymbol{k}} - \varepsilon_{-s\boldsymbol{k}}} \left| \langle \alpha,s,\boldsymbol{k}| \frac{g\mu_B}{2}\sigma_z |\beta,-s,\boldsymbol{k}\rangle \right|^2 \\ &= [-\theta(\varepsilon_F - \varepsilon_{+\boldsymbol{k}}) + \theta(\varepsilon_F - \varepsilon_{-\boldsymbol{k}})] \\ &\quad \times \left(\frac{g\mu_B}{2}\right)^2 \frac{2t^2(\sin^2 k_x a + \sin^2 k_y a)}{\varepsilon_{+\boldsymbol{k}}^3}. \end{aligned} \tag{26}$$

Using these matrix elements, we numerically calculate Eqs. (8) and (9).

Figure 1 shows the spin susceptibility as a function of the Fermi energy ε_F. Around the zero energy where the dispersion relation is linear, the qualitative behavior of the spin susceptibility of the lattice model is the same as the continuum model. The spin susceptibility is almost independent of ε_F. The

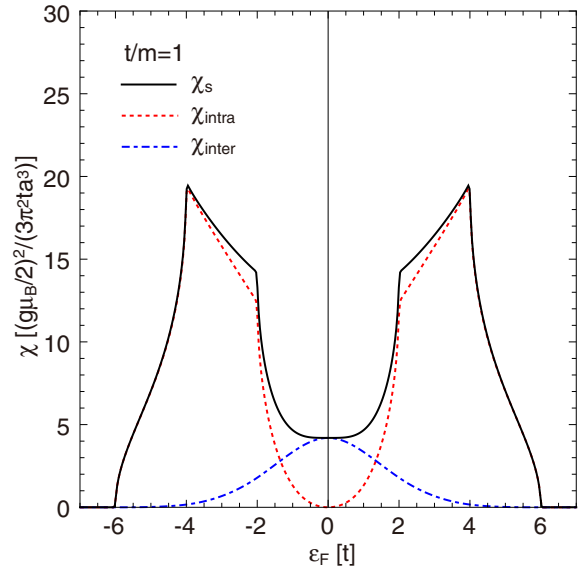

FIG. 1. The spin susceptibility of the lattice model as a function of the Fermi energy. The solid black curve is the spin susceptibility χ_s, the red dashed curve is the intraband contribution $\chi_{\rm intra}$, and the blue dashed curve is the interband contribution $\chi_{\rm inter}$.

intraband contribution vanishes at zero energy and increases off zero energy. The interband contribution has a peak structure at zero energy. In the rest of this section, we discuss the details of the peak structure and address the two remarks in the previous section, the cutoff energy and the offset.

The peak structure is related to the commutation relation between the spin operator and each term in the Hamiltonian. The Hamiltonian is composed of two terms, the first sin term, which does not commute with the spin operator,

$$H_{\rm s} = t\tau_z \sum_{i=x,y,z} \sigma_i \sin k_i a, \tag{27}$$

$$[H_{\rm s},\sigma_z] \neq 0, \tag{28}$$

and the second cos term, which commutes with the spin operator,

$$H_{\rm c} = m\tau_x \sum_{i=x,y,z} (1-\cos k_i a), \tag{29}$$

$$[H_{\rm c},\sigma_z] = 0. \tag{30}$$

Around the Dirac point, the electronic states are mainly described by $H_{\rm s}$, and the interband matrix element is finite. Far from the Dirac point, on the other hand, the electronic states are mainly described by $H_{\rm c}$, and the interband matrix element is negligibly small. This means that the interband contribution Eq. (9) mainly originates from the electronic states around the Dirac point and there is almost no contribution far from the Dirac point. Therefore, the interband contribution has the peak structure and finite value near zero energy. The peak decays far from the Dirac point where the cos term $H_{\rm c}$ is the dominant term in the Hamiltonian $H_{\rm Lattice}$.

Here, we relate the peak width of $\chi_{\rm inter}$ and the cutoff energy $\varepsilon_{\rm c}$, which is introduced in the previous section. In the continuum model, the interband contribution vanishes at the cutoff energy, whereas in the lattice model, the interband contribution decays far from the Dirac point. Therefore, we assume that the cutoff energy corresponds to the peak width and is determined by

$$t\,\sin(k_{\rm c}a/f) = m[1-\cos(k_{\rm c}a/f)], \tag{31}$$

where $k_{\rm c} = \varepsilon_{\rm c}/(\hbar v)$ is the cutoff wave number. This equation means the sin term and the cos term are comparable. In the above equation, we introduce a numerical factor f to fit the spin susceptibility of the continuum and lattice model as discussed following. Solving the above equation, we obtain:

$$k_{\rm c}a = 2f \arctan\left(\frac{t}{m}\right). \tag{32}$$

In Fig. 2, we compare the spin susceptibility of the continuum model and the lattice model. Using Eqs. (22) and (32), the two spin susceptibilities are compared in the same unit. The numerical factor f is determined as

$$f \simeq 1.305, \tag{33}$$

to get quantitative agreement between the two spin susceptibilities at $\varepsilon_{\rm F} = 0$. In the vicinity of zero energy, they are in good agreement with each other. On the other hand, we see the deviation apart from zero energy because of the deviation from the linear dispersion relation.

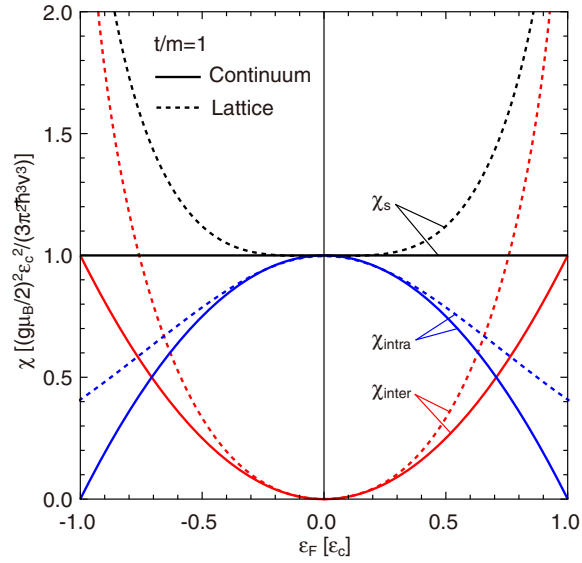

FIG. 2. The spin susceptibility of the continuum model (solid curves) and the lattice model (dashed curves) as a function of the Fermi energy.

Figure 3 compares the spin susceptibility of the continuum model and that of the lattice model at $\varepsilon_{\rm F} = 0$ as a function of t/m. Again we see the quantitative agreement between the two spin susceptibilities. In a condition that $t/m \ll 1$, we can derive an approximate analytical expression for the spin susceptibility of the lattice model. In this condition, the interband matrix elements Eq. (26) are approximated as

$$\frac{2t^2(\sin^2 k_x a + \sin^2 k_y a)}{\varepsilon_{+\boldsymbol{k}}^3} \simeq \frac{2(tka\,\sin\theta_{\boldsymbol{k}})^2}{[(tka)^2 + (mk^2a^2)^2/4]^{3/2}}, \tag{34}$$

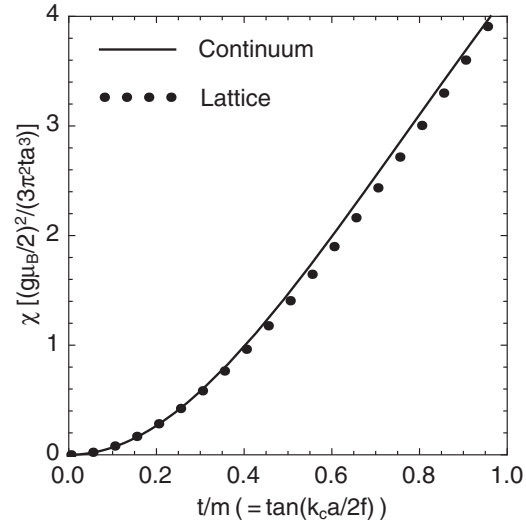

FIG. 3. The spin susceptibility at $\varepsilon_{\rm F} = 0$ as a function of t/m. The solid curve represents the continuum model, and the dotted curve represents the lattice model.

and the spin susceptibility of the lattice model is calculated as

$$\chi_s(\varepsilon_F=0) \simeq \frac{1}{(2\pi)^3}\int_0^\infty k^2 dk \int_0^\pi \sin\theta_{\boldsymbol{k}} d\theta_{\boldsymbol{k}} \int_0^{2\pi} d\phi_{\boldsymbol{k}} \times \left(\frac{g\mu_B}{2}\right)^2 \frac{2(tka\,\sin\theta_{\boldsymbol{k}})^2}{[(tka)^2+(mk^2a^2)^2/4]^{3/2}} = \frac{8}{3\pi^2}\left(\frac{g\mu_B}{2}\right)^2 \frac{t}{m^2a^3}. \quad (35)$$

In the present approximation, Eq. (32) becomes $k_c a \simeq 2f(t/m)$. Consequently, we obtain $\chi_s(\varepsilon_F=0) \propto \varepsilon_c^2/(\hbar v)^3$, which is consistent with Eq. (20).

The discussions presented in this section are summarized as follows. The cutoff energy corresponds to the end of the linear dispersion relation, and we can estimate the spin susceptibility calculated for the continuum model by Eqs. (22) and (32). The constant offset is negligible when the following condition is satisfied:

$$[H_{\rm Lattice},\sigma_z] \simeq 0 \quad (|\boldsymbol{k}| \gg k_c). \quad (36)$$

These criteria are the main results in this paper.

Finally, we mention the effect of the lattice structure. If we consider a more complicated lattice structure than the cubic lattice, the Fermi-energy dependence of the spin susceptibility is qualitatively different from Fig. 1 when the Fermi energy is away from the Dirac point. However, we expect that the discussion given in this section is applicable to the complicated lattice model as long as the low-energy electronic structure is well approximated by the continuum model Eq. (11) and Eq. (36) is satisfied.

We consider the Fu-Kane-Mele model [48,49] as an example of the other lattice models which host the Dirac semimetal. The Hamiltonian is given in the Appendix. Here, we investigate the commutation relation between the spin operator and the Hamiltonian expanded around the Dirac point in the second order of the wave number. Around $X=2\pi/a(0,0,1)$, the expanded Hamiltonian is written as

$$H^X = ta\tau_y k_z + 2\lambda_{SO}a\tau_z(\sigma_x k_x - \sigma_y k_y) + \frac{ta^2}{4}\tau_x[k_z^2 + (k_x+k_y)k_z - k_x k_y]. \quad (37)$$

The k linear terms correspond to the sin term, and the k^2 terms correspond to the cos term in the Wilson-Dirac lattice model. The commutation relation between the k linear terms and the spin operator $\boldsymbol{\sigma}$ is nonzero. On the other hand, the k^2 terms and the spin operator $\boldsymbol{\sigma}$ commute with each other. Therefore, the situation is the same as the Wilson-Dirac lattice model, and the applicability of the conclusion in this section is approximately confirmed.

V. MASSIVE DIRAC FERMION MODEL

In this section, we calculate the spin susceptibility of the massive Dirac Hamiltonian, which can describe an electronic state of topological insulators. In the following calculation, we explicitly set the model parameters based on the first-principles calculation [50] for quantitative estimation of the spin susceptibility.

The electronic state is described by the effective Hamiltonian [50,51]:

$$H_0 = \varepsilon_{\boldsymbol{k}} + M_{\boldsymbol{k}}\tau_z + B_0\tau_y k_z + A_0(\tau_x\sigma_x k_y - \tau_x\sigma_y k_x), \quad (38)$$

where $\varepsilon_{\boldsymbol{k}} = C_0 + C_1 k_z^2 + C_2 k_\parallel^2$, $M_{\boldsymbol{k}} = M_0 + M_1 k_z^2 + M_2 k_\parallel^2$, and $k_\parallel = \sqrt{k_x^2+k_y^2}$. The parameters are taken as $C_0 = -0.0083$ (eV), $C_1 = 5.74$, $C_2 = 30.4$, $M_1 = 6.86$, $M_2 = 44.5$, $A_0 = 3.33$, and $B_0 = 2.26$ (eV Å), which are the parameters for the topological insulator Bi_2Se_3 [50]. The above Hamiltonian describes ordinary insulators, Dirac semimetals, and topological insulators by tuning the parameter M_0, which is related to the strength of the spin-orbit coupling. In the presence of a magnetic field, the Zeeman coupling is given by

$$H_{\rm Zeeman} = -\boldsymbol{M}^{\rm spin}\cdot\boldsymbol{B}, \quad (39)$$

where the spin operators $\boldsymbol{M}^{\rm spin}$ are written as

$$M_x^{\rm spin} = \frac{\mu_B}{2}(g_{xy+}\sigma_x + g_{xy-}\tau_z\sigma_x), \quad (40)$$

$$M_y^{\rm spin} = \frac{\mu_B}{2}(g_{xy+}\sigma_y + g_{xy-}\tau_z\sigma_y), \quad (41)$$

$$M_z^{\rm spin} = \frac{\mu_B}{2}(g_{z+}\sigma_z + g_{z-}\tau_z\sigma_z). \quad (42)$$

We set the effective g factors as $g_{z+} = 10.65$, $g_{z-} = 14.75$, $g_{xy+} = -0.34$, and $g_{xy-} = 4.46$, which are also the parameters for the topological insulator Bi_2Se_3 [50]. In this model, there are two kinds of Zeeman terms, "orbital-independent" term (σ_α) and "orbital-dependent" term ($\tau_z\sigma_\alpha$) [52]. This originates from the nonequality of the effective g factors in the two orbitals. In the magnetically doped topological insulators, the exchange coupling also has the similar terms, i.e., orbital-independent and orbital-dependent terms [53]. Therefore, we note that the consideration of these terms is important also in the magnetic phase transition. The eigenstates of the above Hamiltonian are given by

$$|1,+,\boldsymbol{k}\rangle = \frac{1}{\sqrt{2\varepsilon_{+\boldsymbol{k}}^{(0)}(\varepsilon_{+\boldsymbol{k}}^{(0)}+M_{\boldsymbol{k}})}}\begin{pmatrix}\varepsilon_{+\boldsymbol{k}}^{(0)}+M_{\boldsymbol{k}}\\0\\iB_0k_z\\-iA_0k_+\end{pmatrix}, \quad (43)$$

$$|2,+,\boldsymbol{k}\rangle = \frac{1}{\sqrt{2\varepsilon_{+\boldsymbol{k}}^{(0)}(\varepsilon_{+\boldsymbol{k}}^{(0)}+M_{\boldsymbol{k}})}}\begin{pmatrix}0\\\varepsilon_{+\boldsymbol{k}}^{(0)}+M_{\boldsymbol{k}}\\iA_0k_-\\iB_0k_z\end{pmatrix}, \quad (44)$$

$$|1,-,\boldsymbol{k}\rangle = \frac{1}{\sqrt{2\varepsilon_{-\boldsymbol{k}}^{(0)}(\varepsilon_{-\boldsymbol{k}}^{(0)}-M_{\boldsymbol{k}})}}\begin{pmatrix}-iB_0k_z\\-iA_0k_+\\\varepsilon_{-\boldsymbol{k}}^{(0)}-M_{\boldsymbol{k}}\\0\end{pmatrix}, \quad (45)$$

$$|2,-,\boldsymbol{k}\rangle = \frac{1}{\sqrt{2\varepsilon_{-\boldsymbol{k}}^{(0)}(\varepsilon_{-\boldsymbol{k}}^{(0)}-M_{\boldsymbol{k}})}}\begin{pmatrix}iA_0k_-\\-iB_0k_z\\0\\\varepsilon_{-\boldsymbol{k}}^{(0)}-M_{\boldsymbol{k}}\end{pmatrix}, \quad (46)$$

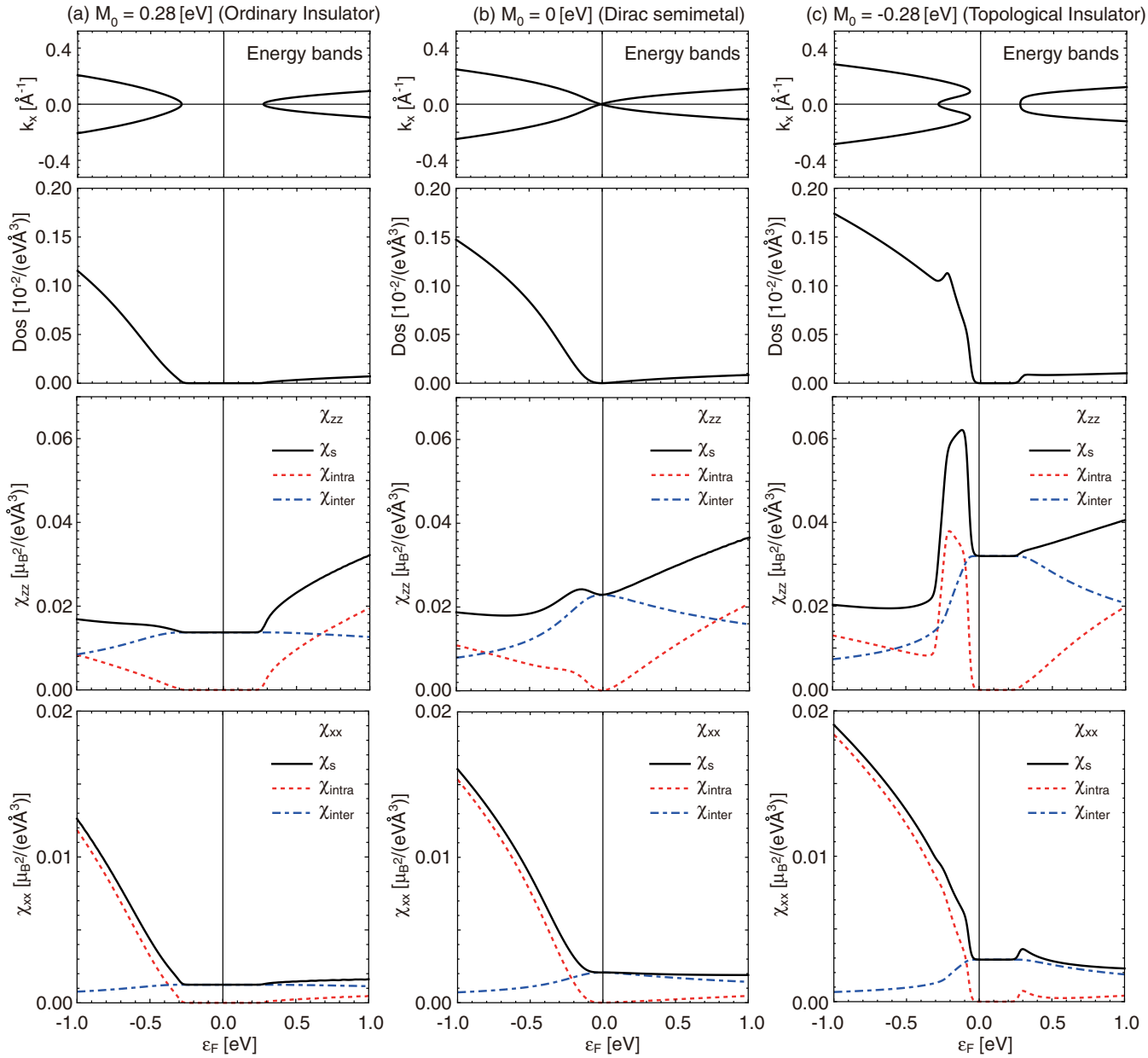

FIG. 4. The density of states and the spin susceptibility of (a) an ordinary insulator, (b) a Dirac semimetal, and (c) a topological insulator as a function of the Fermi energy. The top panels show the energy bands where we set $k_y = k_z = 0$.

where $k_\pm = k_x \pm ik_y$ and the energy for $|n,s,\boldsymbol{k}\rangle$ is given by

$$\varepsilon_{s\boldsymbol{k}} = \varepsilon_{\boldsymbol{k}} + \varepsilon^{(0)}_{s\boldsymbol{k}}, \tag{47}$$

$$\varepsilon^{(0)}_{s\boldsymbol{k}} = s\sqrt{A_0^2 k_\parallel^2 + B_0^2 k_z^2 + M_{\boldsymbol{k}}^2}. \tag{48}$$

Based on the symmetry, the spin susceptibility along the x axis and the y axis exhibit the same behavior. Therefore, we calculate the spin susceptibility along the x axis and the z axis. The intraband matrix elements are calculated as

$$\sum_{nm} \delta(\varepsilon_{s\boldsymbol{k}} - \varepsilon_{\rm F}) \left|\langle n,s,\boldsymbol{k}|M_x^{\rm spin}|m,s,\boldsymbol{k}\rangle\right|^2 = \delta(\varepsilon_{s\boldsymbol{k}} - \varepsilon_{\rm F}) \left(\frac{\mu_{\rm B}}{2}\right)^2 \frac{2\left[g_{xy+}^2\left(\varepsilon^{(0)2}_{s\boldsymbol{k}} - A_0^2 k_x^2\right) + 2g_{xy+}g_{xy-}\varepsilon^{(0)}_{s\boldsymbol{k}} M_{\boldsymbol{k}} + g_{xy-}^2\left(A_0^2 k_x^2 + M_{\boldsymbol{k}}^2\right)\right]}{\varepsilon^{(0)2}_{s\boldsymbol{k}}}, \tag{49}$$

and

$$\sum_{nm}\delta(\varepsilon_{s\boldsymbol{k}}-\varepsilon_{\rm F})\left|\langle n,s,\boldsymbol{k}|M_z^{\rm spin}|m,s,\boldsymbol{k}\rangle\right|^2=\delta(\varepsilon_{s\boldsymbol{k}}-\varepsilon_{\rm F})\left(\frac{\mu_{\rm B}}{2}\right)^2\frac{2\left[g_{z+}^2\left(B_0^2k_z^2+M_{\boldsymbol{k}}^2\right)+2g_{z+}g_{z-}\varepsilon_{s\boldsymbol{k}}^{(0)}M_{\boldsymbol{k}}+g_{z-}^2\left(\varepsilon_{s\boldsymbol{k}}^{(0)2}-B_0^2k_z^2\right)\right]}{\varepsilon_{s\boldsymbol{k}}^{(0)2}}. \tag{50}$$

The interband matrix elements are

$$\sum_{nms}\frac{-\theta(\varepsilon_{\rm F}-\varepsilon_{s\boldsymbol{k}})+\theta(\varepsilon_{\rm F}-\varepsilon_{-s\boldsymbol{k}})}{\varepsilon_{s\boldsymbol{k}}-\varepsilon_{-s\boldsymbol{k}}}\left|\langle n,s,\boldsymbol{k}|M_x^{\rm spin}|m,-s,\boldsymbol{k}\rangle\right|^2$$
$$=\left[-\theta(\varepsilon_{\rm F}-\varepsilon_{+\boldsymbol{k}})+\theta(\varepsilon_{\rm F}-\varepsilon_{-\boldsymbol{k}})\right]\left(\frac{\mu_{\rm B}}{2}\right)^2\frac{2\left[g_{xy+}^2A_0^2k_x^2+g_{xy-}^2\left(A_0^2k_y^2+B_0^2k_z^2\right)\right]}{\varepsilon_{+\boldsymbol{k}}^{(0)3}}, \tag{51}$$

and

$$\sum_{nms}\frac{-\theta(\varepsilon_{\rm F}-\varepsilon_{s\boldsymbol{k}})+\theta(\varepsilon_{\rm F}-\varepsilon_{-s\boldsymbol{k}})}{\varepsilon_{s\boldsymbol{k}}-\varepsilon_{-s\boldsymbol{k}}}\left|\langle n,s,\boldsymbol{k}|M_z^{\rm spin}|m,-s,\boldsymbol{k}\rangle\right|^2$$
$$=\left[-\theta(\varepsilon_{\rm F}-\varepsilon_{+\boldsymbol{k}})+\theta(\varepsilon_{\rm F}-\varepsilon_{-\boldsymbol{k}})\right]\left(\frac{\mu_{\rm B}}{2}\right)^2\frac{2\left[g_{z+}^2A_0^2\left(k_x^2+k_y^2\right)+g_{z-}^2B_0^2k_z^2\right]}{\varepsilon_{+\boldsymbol{k}}^{(0)3}}. \tag{52}$$

The spin susceptibility is numerically calculated in a similar manner to the previous sections. Figure 4 shows the density of states and the spin susceptibility as a function of the Fermi energy $\varepsilon_{\rm F}$. The top panels in Fig. 4 show the energy bands. We calculate them for three parameters (a) $M_0=0.28$ (eV) (ordinary insulator), (b) $M_0=0.0$ (eV) (Dirac semimetal), and (c) $M_0=-0.28$ (eV) (topological insulator). Even in the current effective model, which includes the anisotropy and the two types of the Zeeman term, the qualitative behavior of the interband contribution is similar to that of the previous models. The interband contribution takes the maximum value in the energy gap or at the band touching point where the density of states vanishes. Away from the zero energy, the interband contribution monotonically decreases in a similar manner to the previous model. On the other hand, the intraband contribution behaves in a slightly different manner from the previous model. In the previous models, the intraband contribution is proportional to the density of states. In the current model, the density of states of the valence band is larger than the conduction band, but the intraband contributions for χ_{zz} in the valence and conduction bands are comparable. This originates from the cross term of g_{z+} and g_{z-} in Eq. (50). The cross term gives a positive contribution in the conduction band and a negative contribution in the valence band. Consequently, the intraband contributions in the valence and conduction bands are comparable. On the other hand, the intraband contributions for χ_{xx} in the valence and conduction bands are not comparable. This is because the effective g factors g_{xy+} and g_{xy-} have opposite signs so that the cross term does not work as in the case of χ_{zz}, where g_{z+} and g_{z-} have the same signs. In Fig. 4(c), the topological insulator case, there is another important feature. The intraband contribution for χ_{zz} exhibits a peak structure in the valence band. The peak width corresponds to the band inverted region. On the other hand, there is no peak structure in χ_{xx}.

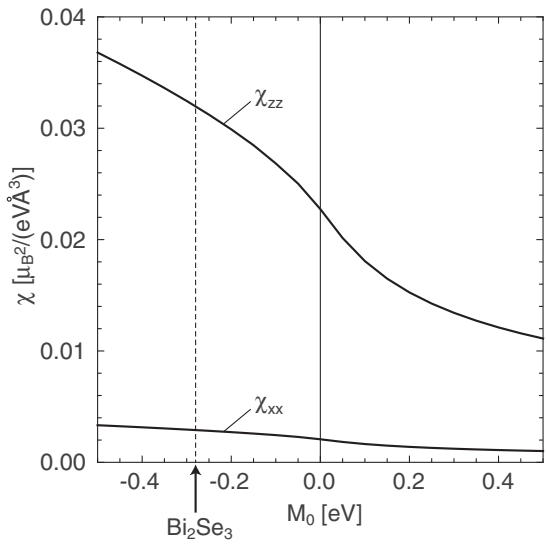

FIG. 5. The spin susceptibility of the x and z directions in the energy gap as a function of M_0. The vertical dashed line corresponds to the value of M_0 for Bi_2Se_3.

In Fig. 5, we plot the spin susceptibility in the energy gap as a function of M_0. The spin susceptibility increases with the decrease in M_0, which means the increase in the spin-orbit coupling [28,34]. The strong spin-orbit coupling gives the large interband contribution. χ_{zz} is much larger than χ_{xx} because the effective g factors for the z direction are much larger than the x direction.

VI. CONCLUSION

We have studied the spin susceptibility of the Dirac semimetals. The spin susceptibility is calculated for the massless Dirac continuum model and the Wilson-Dirac lattice model. In the massless Dirac continuum model, we have to introduce the cutoff energy $\varepsilon_{\rm c}$ in order to regularize the

integration. The spin susceptibility is independent of the Fermi-energy ε_F and proportional to ε_c^2. We find that the cutoff energy is appropriately determined and related to the same parameters of the lattice model. The cutoff energy corresponds to the energy where the band dispersion deviates from the linear dispersion relation. The spin susceptibility of the lattice model is in quantitatively good agreement with the massless Dirac continuum model. We also calculate the spin susceptibility of massive Dirac fermions with the Zeeman coupling including the orbital-dependent term and the orbital-independent term. The spin susceptibility along the z axis is enhanced in the conduction band because of the existence of two types of the Zeeman term and has the peak structure in the band inverted region, which are not observed in the spin susceptibility along the x axis. In this paper, we consider noninteracting Dirac fermions. Most of the Dirac-Weyl semimetals are realized in s- and p-electron systems. Therefore, the electron-electron interaction is negligible, and this paper is applicable to them. On the other hand, the electron-electron interaction is important in strongly correlated d-electron systems [54,55], such as the pyrochlore iridates [5,6]. The effect of the electron-electron interaction for the spin susceptibility is left for the future.

ACKNOWLEDGMENTS

The authors thank Y. Araki and M. Oshikawa for helpful discussions. This work was supported by Kakenhi Grants-in-Aid (Grants No. JP15H05854 and No. JP17K05485) from the Japan Society for the Promotion of Science (JSPS).

APPENDIX: THE FU-KANE-MELE MODEL

In this Appendix, we introduce the Fu-Kane-Mele model, which is the tight-binding model on the diamond lattice with the spin-orbit coupling. The Hamiltonian is given as

$$H = t\sum_{\langle ij\rangle} c_i^\dagger c_j + i(4\lambda_{\rm SO}/a^2)\sum_{\langle\langle ij\rangle\rangle} c_i^\dagger \boldsymbol{\sigma}\cdot\left(\boldsymbol{d}_{ij}^1\times\boldsymbol{d}_{ij}^2\right)c_j. \quad \text{(A1)}$$

$c_i^\dagger$ and c_i are creation and annihilation operators for the electron on the i site. The first term is a nearest-neighbor hopping term with a hopping parameter t. The second term connects second neighbors with a spin-dependent amplitude. $\lambda_{\rm SO}$ represents the strength of the spin-orbit coupling. $\boldsymbol{d}_{ij}^{1,2}$ are the two nearest-neighbor bond vectors traversed between sites i and j. a is the lattice constant. The Hamiltonian in k space is written as

$$H(\boldsymbol{k}) = \sum_{a=1}^{5} d_a(\boldsymbol{k})\Gamma^a, \quad \text{(A2)}$$

where

$$\Gamma^{(1-5)} = (\tau_x,\tau_y,\tau_z\sigma_x,\tau_z\sigma_y,\tau_z\sigma_z), \quad \text{(A3)}$$

and

$$\begin{aligned} d_1 &= t + t(\cos x_1 + \cos x_2 + \cos x_3),\\ d_2 &= t(\sin x_1 + \sin x_2 + \sin x_3),\\ d_3 &= \lambda_{\rm SO}[\sin x_2 - \sin x_3 - \sin(x_2 - x_1) + \sin(x_3 - x_1)],\\ d_4 &= \lambda_{\rm SO}[\sin x_3 - \sin x_1 - \sin(x_3 - x_2) + \sin(x_1 - x_2)],\\ d_5 &= \lambda_{\rm SO}[\sin x_1 - \sin x_2 - \sin(x_1 - x_3) + \sin(x_2 - x_3)], \end{aligned} \quad \text{(A4)}$$

where $x_i = \boldsymbol{k}\cdot\boldsymbol{a}_i$, $\boldsymbol{a}_1 = a(0,1,1)/2$, $\boldsymbol{a}_2 = a(1,0,1)/2$, and $\boldsymbol{a}_3 = a(1,1,0)/2$. In this model, there are three Dirac points at the three inequivalent X points on the 100, 010, and 001 faces of the Brillouin zone.

[1] S. M. Young, S. Zaheer, J. C. Y. Teo, C. L. Kane, E. J. Mele, and A. M. Rappe, Phys. Rev. Lett. **108**, 140405 (2012).
[2] Z. Wang, Y. Sun, X.-Q. Chen, C. Franchini, G. Xu, H. Weng, X. Dai, and Z. Fang, Phys. Rev. B **85**, 195320 (2012).
[3] S. Murakami, New J. Phys. **9**, 356 (2007).
[4] A. A. Burkov and L. Balents, Phys. Rev. Lett. **107**, 127205 (2011).
[5] X. Wan, A. M. Turner, A. Vishwanath, and S. Y. Savrasov, Phys. Rev. B **83**, 205101 (2011).
[6] W. Witczak-Krempa and Y. B. Kim, Phys. Rev. B **85**, 045124 (2012).
[7] A. A. Burkov, M. D. Hook, and L. Balents, Phys. Rev. B **84**, 235126 (2011).
[8] M. Phillips and V. Aji, Phys. Rev. B **90**, 115111 (2014).
[9] Y. Kim, B. J. Wieder, C. L. Kane, and A. M. Rappe, Phys. Rev. Lett. **115**, 036806 (2015).
[10] R. Yu, H. Weng, Z. Fang, X. Dai, and X. Hu, Phys. Rev. Lett. **115**, 036807 (2015).
[11] Z. Liu, B. Zhou, Y. Zhang, Z. Wang, H. Weng, D. Prabhakaran, S.-K. Mo, Z. Shen, Z. Fang, X. Dai *et al.*, Science **343**, 864 (2014).
[12] M. Neupane, S.-Y. Xu, R. Sankar, N. Alidoust, G. Bian, C. Liu, I. Belopolski, T.-R. Chang, H.-T. Jeng, H. Lin *et al.*, Nat. Commun. **5**, 3786 (2014).
[13] S. Borisenko, Q. Gibson, D. Evtushinsky, V. Zabolotnyy, B. Büchner, and R. J. Cava, Phys. Rev. Lett. **113**, 027603 (2014).
[14] S.-Y. Xu, I. Belopolski, N. Alidoust, M. Neupane, G. Bian, C. Zhang, R. Sankar, G. Chang, Z. Yuan, C.-C. Lee *et al.*, Science **349**, 613 (2015).
[15] L. Lu, Z. Wang, D. Ye, L. Ran, L. Fu, J. D. Joannopoulos, and M. Soljacic, Science **349**, 622 (2015).
[16] B. Lv, H. Weng, B. Fu, X. Wang, H. Miao, J. Ma, P. Richard, X. Huang, L. Zhao, G. Chen *et al.*, Phys. Rev. X **5**, 031013 (2015).
[17] K. Deng, G. Wan, P. Deng, K. Zhang, S. Ding, E. Wang, M. Yan, H. Huang, H. Zhang, Z. Xu *et al.*, Nat. Phys. **12**, 1105 (2016).
[18] S. Nakatsuji, N. Kiyohara, and T. Higo, Nature (London) **527**, 212 (2015).
[19] A. K. Nayak, J. E. Fischer, Y. Sun, B. Yan, J. Karel, A. C. Komarek, C. Shekhar, N. Kumar, W. Schnelle, J. Kübler *et al.*, Sci. Adv. **2**, e1501870 (2016).
[20] E. Liu, Y. Sun, L. Müechler, A. Sun, L. Jiao, J. Kroder, V. Süß, H. Borrmann, W. Wang, W. Schnelle *et al.*, arXiv:1712.06722.
[21] D. Kurebayashi and K. Nomura, J. Phys. Soc. Jpn. **83**, 063709 (2014).
[22] Z. Wang, M. G. Vergniory, S. Kushwaha, M. Hirschberger, E. V. Chulkov, A. Ernst, N. P. Ong, R. J. Cava, and B. A. Bernevig, Phys. Rev. Lett. **117**, 236401 (2016).
[23] N. Ito and K. Nomura, J. Phys. Soc. Jpn. **86**, 063703 (2017).

[24] H. Yang, Y. Sun, Y. Zhang, W.-J. Shi, S. S. Parkin, and B. Yan, New J. Phys. **19**, 015008 (2017).
[25] Y. J. Jin, R. Wang, Z. J. Chen, J. Z. Zhao, Y. J. Zhao, and H. Xu, Phys. Rev. B **96**, 201102(R) (2017).
[26] Q. Xu, E. Liu, W. Shi, L. Muechler, C. Felser, and Y. Sun, arXiv:1801.00136.
[27] G. Y. Cho, arXiv:1110.1939.
[28] R. Yu, W. Zhang, H.-J. Zhang, S.-C. Zhang, X. Dai, and Z. Fang, Science **329**, 61 (2010).
[29] C.-X. Liu, P. Ye, and X.-L. Qi, Phys. Rev. B **87**, 235306 (2013).
[30] Y. Chen, J.-H. Chu, J. Analytis, Z. Liu, K. Igarashi, H.-H. Kuo, X. Qi, S.-K. Mo, R. Moore, D. Lu *et al.*, Science **329**, 659 (2010).
[31] L. A. Wray, S.-Y. Xu, Y. Xia, D. Hsieh, A. V. Fedorov, Y. San Hor, R. J. Cava, A. Bansil, H. Lin, and M. Z. Hasan, Nat. Phys. **7**, 32 (2011).
[32] M. Liu, J. Zhang, C.-Z. Chang, Z. Zhang, X. Feng, K. Li, K. He, L.-l. Wang, X. Chen, X. Dai *et al.*, Phys. Rev. Lett. **108**, 036805 (2012).
[33] D. Zhang, A. Richardella, D. W. Rench, S.-Y. Xu, A. Kandala, T. C. Flanagan, H. Beidenkopf, A. L. Yeats, B. B. Buckley, P. V. Klimov *et al.*, Phys. Rev. B **86**, 205127 (2012).
[34] J. Zhang, C.-Z. Chang, P. Tang, Z. Zhang, X. Feng, K. Li, L.-l. Wang, X. Chen, C. Liu, W. Duan *et al.*, Science **339**, 1582 (2013).
[35] C.-Z. Chang, J. Zhang, X. Feng, J. Shen, Z. Zhang, M. Guo, K. Li, Y. Ou, P. Wei, L.-L. Wang *et al.*, Science **340**, 167 (2013).
[36] C.-Z. Chang, J. Zhang, M. Liu, Z. Zhang, X. Feng, K. Li, L.-L. Wang, X. Chen, X. Dai, Z. Fang *et al.*, Adv. Mater. **25**, 1065 (2013).
[37] H. Fukuyama and R. Kubo, J. Phys. Soc. Jpn. **28**, 570 (1970).
[38] Y. Fuseya, M. Ogata, and H. Fukuyama, Phys. Rev. Lett. **102**, 066601 (2009).
[39] M. Koshino and T. Ando, Phys. Rev. B **81**, 195431 (2010).
[40] Y. Fuseya, M. Ogata, and H. Fukuyama, J. Phys. Soc. Jpn. **81**, 093704 (2012).
[41] M. Koshino and I. F. Hizbullah, Phys. Rev. B **93**, 045201 (2016).
[42] L. M. Roth, B. Lax, and S. Zwerdling, Phys. Rev. **114**, 90 (1959).
[43] J. Zhou and H.-R. Chang, Phys. Rev. B **97**, 075202 (2018).
[44] A. Thakur, K. Sadhukhan, and A. Agarwal, Phys. Rev. B **97**, 035403 (2018).
[45] M. M. Vazifeh and M. Franz, Phys. Rev. B **86**, 045451 (2012).
[46] L. Zhao, H. Deng, I. Korzhovska, Z. Chen, M. Konczykowski, A. Hruban, V. Oganesyan, and L. Krusin-Elbaum, Nature Mater. **13**, 580 (2014).
[47] R. Lundgren and J. Maciejko, Phys. Rev. Lett. **115**, 066401 (2015).
[48] L. Fu, C. L. Kane, and E. J. Mele, Phys. Rev. Lett. **98**, 106803 (2007).
[49] L. Fu and C. L. Kane, Phys. Rev. B **76**, 045302 (2007).
[50] C.-X. Liu, X.-L. Qi, H.J. Zhang, X. Dai, Z. Fang, and S.-C. Zhang, Phys. Rev. B **82**, 045122 (2010).
[51] H. Zhang, C.-X. Liu, X.-L. Qi, X. Dai, Z. Fang, and S.-C. Zhang, Nat. Phys. **5**, 438 (2009).
[52] R. Nakai and K. Nomura, Phys. Rev. B **93**, 214434 (2016).
[53] R. Wakatsuki, M. Ezawa, and N. Nagaosa, Sci. Rep. **5**, 13638 (2015).
[54] A. Sekine and K. Nomura, J. Phys. Soc. Jpn. **83**, 094710 (2014).
[55] A. Sekine and K. Nomura, Phys. Rev. B **90**, 075137 (2014).